New Journal of Physics
The open-access journal for physics

Electron–phonon coupling at surfaces and interfaces

Ph Hofmann[1], I Yu Sklyadneva[2,3], E D L Rienks[4] and E V Chulkov[2,5]

[1] Institute for Storage Ring Facilities and Interdisciplinary Nanoscience Center (iNANO), Aarhus University, 8000 Aarhus C, Denmark
[2] Donostia International Physics Center (DIPC), P. de Manuel Lardizabal, 4, 20018, San Sebastián, Basque Country, Spain
[3] Institute of Strength Physics and Materials Science, RAS, pr. Academicheskii 2/1, 634021, Tomsk, Russia
[4] Institute for Storage Ring Facilities and Interdisciplinary Nanoscience Center, University of Aarhus, 8000 Aarhus C, Denmark
[5] Departamento de Física de Materiales, Facultad de Ciencias Químicas, UPV/EHU and Centro Mixto CSIC-UPV/EHU, Apdo. 1072, 20080 San Sebastián, Basque Country, Spain
E-mail: evguenivladimirovich.tchoulkov@ehu.es

New Journal of Physics **11** (2009) 125005 (29pp)
Received 9 May 2009
Published 11 December 2009
Online at http://www.njp.org/
doi:10.1088/1367-2630/11/12/125005

Abstract. Over the recent years, electronic surface states have been used for a detailed spectroscopic study of the electron–phonon (e–ph) interaction, both experimentally and theoretically. This review discusses the basic physics of e–ph coupling and how information can be obtained from angle-resolved photoemission experiments and first principles calculations. Several recent results for clean and adsorbate-covered surfaces, quantum wells and free-standing monolayers are also discussed.

© IOP Publishing Ltd and Deutsche Physikalische Gesellschaft

Contents

1. Introduction

Many-body effects and their interplay are at the heart of some of the most interesting problems in current condensed matter physics, and frequently the simultaneous presence of different effects is found in complex materials. The electron–phonon (e–ph) interaction is one such effect that limits the lifetime of excited electrons (or holes) and has long been studied because of its role in many phenomena, from electrical conductivity to electronic heat capacity and BCS-type superconductivity. Several experimental techniques such as tunneling spectroscopy or heat capacity measurements have provided information on the e–ph coupling strength averaged over the bulk Fermi surface of metals [44].

More recently, interest in the e–ph coupling has been revived for several reasons. E–ph interaction is a prominent member of the family of many-body interactions that are found in complex materials like the high-temperature cuprate superconductors. In fact, e–ph coupling has been proposed to be an important ingredient for high-temperature superconductivity [72] but at present spectroscopic evidence merely exist for a strong electron–boson coupling that is not necessarily caused by the e–ph interaction [3].

Experimentally, recent advances in angle-resolved photoemission (ARPES) have opened the opportunity for a study of many-body effects in unprecedented detail. Most importantly, studies are not confined to averages over the Fermi surface but detailed information about the energy and k dependence of the interaction has come in reach. This permits us, for instance, to establish the symmetry of the superconducting gap in novel superconductors [4, 26].

The e–ph interaction stands out as a fundamental many-body process that can be tested by both experimental and theoretical methods. Much has been learned by studying the e–ph coupling on carefully chosen electronic surface states, for which good arguments can be made for the e–ph interaction to be the *only* many-body effect giving rise to a bosonic spectroscopic signature. Surface states have also played an important role because they have, as do the states in the cuprates, a merely two-dimensional (2D) dispersion, an essential prerequisite for the analysis of ARPES data.

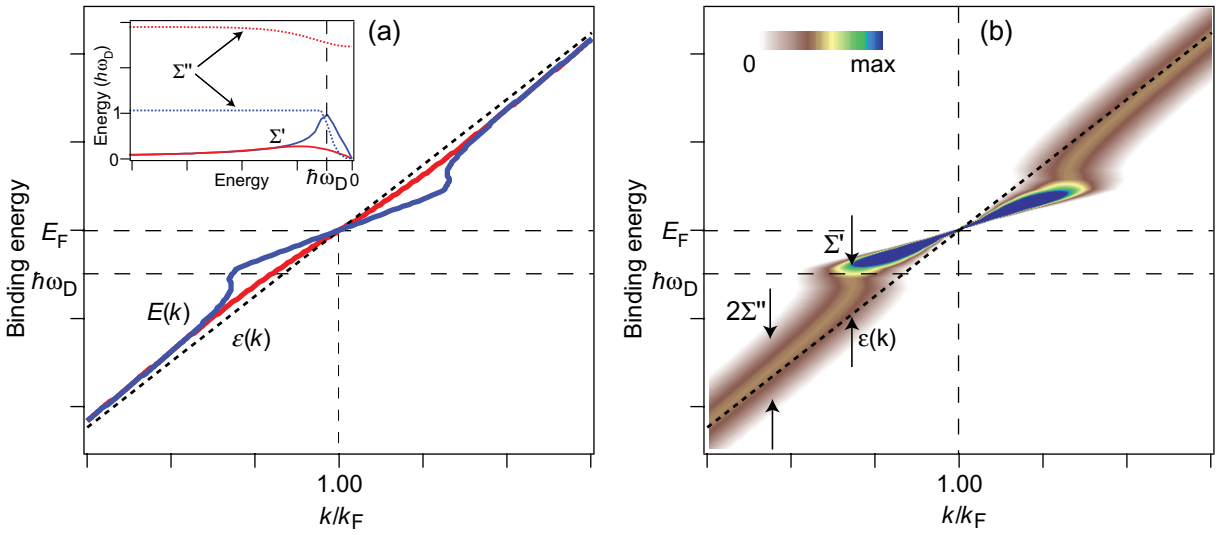

Figure 1. (a) Renormalization of the electronic dispersion close to the Fermi energy (schematic). The dashed line is the bare dispersion $\epsilon(k)$; the solid line is the renormalized dispersion $E(k)$ for a low temperature (blue) and a higher temperature (red). Inset: real and imaginary parts of the complex self-energy for the e–ph coupling, Σ' and Σ'' for a low temperature (blue) and a higher temperature (red). (b) Spectral function $\mathcal{A}(\omega, \vec{k}, T)$ at a low temperature showing the sharpening of the quasi-particle peak near E_F. The arrows indicate how Σ' and Σ'' correspond to the renormalization of the dispersion and the finite width of the peak, respectively. The inset bar gives the color scale.

In the most simple picture, the e–ph coupling changes the dispersion and the lifetime of the electronic states in a material. This situation is illustrated in figure 1(a). Very close to the Fermi level, within a typical phonon energy $\hbar\omega_D$, the dispersion is renormalized such that it is flatter at the Fermi energy. Consequently, the effective mass of the electrons at the Fermi level and the density of states (DOS) are increased [44]. The increase of the effective mass is described by the e–ph mass enhancement parameter λ such that $m^* = m_0(1+\lambda)$, where m^* and m_0 are the effective masses with and without e–ph interaction, respectively.

The effect of the e–ph coupling on the dispersion and lifetime of the states can be expressed by the complex self-energy Σ, where the real part Σ' renormalizes the dispersion and the states acquire a finite lifetime τ through the imaginary part Σ''. In this context, both $\Sigma'' = \hbar/2\tau$ and the inverse lifetime $\Gamma = \hbar/\tau$ are frequently used. All the closely related quantities Σ', Σ'', Γ and τ can be obtained from the spectral function $A(\omega, \vec{k}, T)$, which is defined later on in this paper, but for now can be taken to be proportional to the photoemission intensity in ARPES. Figure 1(b) shows a plot of the spectral function at low temperature and indicates how Σ' and Σ'' (or Γ) give rise to a renormalization and broadening, respectively.

Typical results for Σ' and Σ'' (calculated in the Debye model) are given in the inset of figure 1(a). Σ' is small except for energies very close to the Fermi level. Σ'' is changing rapidly close to the Fermi level and is constant at higher energies. Σ' vanishes exactly at E_F such that the Fermi surface is not affected by the interaction. Σ'' only vanishes at E_F for zero temperature. Both are related by a Hilbert transformation, i.e. from a spectroscopic point of view it is sufficient to determine either Σ' or Σ''.

The lifetime τ, inverse lifetime Γ or the imaginary part of the self-energy Σ'' are all essentially the same quantity, describing the decay of excited electrons or holes. In this paper, we are primarily interested in a decay that involves e–ph coupling but we briefly discuss other scattering mechanisms as well, since they will eventually contribute to the total Γ, and since we have to single out the e–ph contribution. In paramagnetic metals, Γ has three contributions, e–ph, electron–electron (e–e) scattering and electron–defect (e–df) interactions [18]. These contributions are additive such that

$$\Gamma = \hbar/\tau = \Gamma_{\text{e–df}} + \Gamma_{\text{e–e}} + \Gamma_{\text{e–ph}}. \tag{1}$$

$\Gamma_{\text{e–df}}$ takes into account elastic scattering processes by defects that limit the mean-free path of a carrier. $\Gamma_{\text{e–df}}$ is usually not strongly energy or temperature dependent and thus acts as a mere offset to Γ. Notice, however, that while the defect scattering strength might not be temperature dependent, the number of defects is: defects can be thermally excited at elevated temperatures and this can contribute to an increase of $\Gamma_{\text{e–df}}$ [62, 106]. Often the defect scattering can be suppressed in experiments such as scanning tunneling spectroscopy measurements [30, 67, 70] or time-resolved two-photon-photoemission [30, 54, 116]. It can also be strongly reduced in photoemission spectroscopy studies [30, 96].

$\Gamma_{\text{e–e}}$, the contribution from the predominantly inelastic e–e scattering, includes several decay channels related to charge-density, spin-density, singlet-pair and triplet-pair fluctuations [30]. $\Gamma_{\text{e–e}}$ is energy-dependent: it increases for higher binding energies because the phase space for inelastic e–e scattering is extended. The temperature dependence of $\Gamma_{\text{e–e}}$, on the other hand, is usually very small, in sharp contrast to $\Gamma_{\text{e–ph}}$, which increases at high temperatures because of the increased probability of phonon excitations. At sufficiently low temperatures, in the absence of defects and for large excitation energies, the e–e scattering is the most important process that limits the excitation lifetime. However, close to the Fermi level and in particular for high temperatures, $\Gamma_{\text{e–e}}$ can become smaller than $\Gamma_{\text{e–ph}}$ [18, 19, 30, 34, 48, 49, 108].

An important result from these considerations is that in many situations, the e–ph contribution is the only one to Γ, see equation (1), with a significant temperature dependence and this can be exploited to single out the e–ph part from the other contributions experimentally.

In the following sections, we discuss how the e–ph interaction can be described theoretically, how information about it can be extracted from experimental data, and we discuss a few selected cases. We do not attempt to present a complete overview on the current status of the field but rather focus on some historically and didactically valuable examples. Particular emphasis will be put on cases for which both experimental data and *ab initio* calculations are available.

2. Calculation of the e–ph coupling strength

A basic quantity of the e–ph interaction is the e–ph matrix that gives the probability of electron scattering from an initial electron state (i) with momentum $\mathbf{k}$ to a final electron state (f) by a phonon with momentum $\mathbf{q}$ and mode index ν:

$$g^{\text{i,f}}(\mathbf{k}, \mathbf{q}, \nu) = \sqrt{\frac{1}{2M\omega_{\mathbf{q},\nu}}} \langle \Psi_{\mathbf{ki}} |\, \hat{\varepsilon}_{\mathbf{q},\nu} \cdot \delta V^{\text{SCF}}_{\mathbf{q},\nu} |\, \Psi_{\mathbf{k+qf}} \rangle. \tag{2}$$

Here, M is the atomic mass, $\Psi_{\mathbf{ki}}$ and $\Psi_{\mathbf{k+qf}}$ are the electronic wavefunctions for the initial and final states, respectively. $\delta V^{\text{SCF}}_{\mathbf{q},\nu}$ gives the gradient of the self-consistent potential with respect to

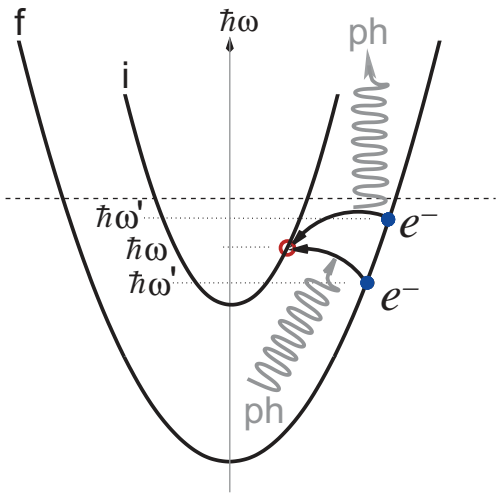

Figure 2. Phonon-mediated interband scattering from a filled circle (final state of the hole) to the open circle (initial state of the hole) by phonon emission and phonon absorption. Figure adapted from [49].

the atomic displacements induced by the phonon mode ($\mathbf{q}$, ν) with frequency $\omega_{\mathbf{q},\nu}$ and phonon polarization vector $\hat{\varepsilon}_{\mathbf{q},\nu}$. Such phonon-mediated interband scattering is shown schematically in figure 2.

The effectiveness of phonons with energy $\hbar\omega$ to scatter electrons is expressed in terms of the Eliashberg coupling function, $\alpha^2F(\omega)$. If the initial electron energy ϵ_i and momentum $\mathbf{k}$ are fixed, the corresponding state-dependent Eliashberg function gives the e–ph coupling between the initial state and all other final states (ϵ_f), which differ in energy by $\hbar\omega$ due to phonon emission (E) or absorption (A) processes:

$$\alpha^2F^{\mathrm{E(A)}}(\epsilon_\mathrm{i}, \mathbf{k}; \omega) = \sum_{\mathbf{q},\nu,\mathrm{f}} \delta(\epsilon_\mathrm{i} - \epsilon_\mathrm{f} \mp \omega_{\mathbf{q},\nu})|\mathrm{g}^{\mathrm{i,f}}(\mathbf{k}, \mathbf{q}, \nu)|^2\delta(\omega - \omega_{\mathbf{q},\nu}). \tag{3}$$

The '−' and '+' signs in the delta function with electron energies correspond to a phonon emission and absorption, respectively. The sum is carried out over final electron states (f) and all phonon modes ($\mathbf{q}$, ν). As one can see from equation (3), $\alpha^2F(\omega)$ is nothing else than the phonon DOS weighted by the e–ph coupling.

Figure 3 shows an example of the Eliashberg function. It was calculated for a hole state in the $\bar{\Gamma}$ symmetry point on the Cu(111) surface state [34]. The figure also shows the calculated phonon dispersion, in which the surface-localized Rayleigh mode is clearly identified as split-off below the bulk continuum around the $\bar{M}$ point. This mode contributes significantly to the Eliashberg function. Its contribution has been singled out by the dashed line in $\alpha^2F(\omega)$.

While the e–ph mass enhancement parameter's original definition is related to the overall mass enhancement at the Fermi surface, a more spectroscopic interpretation of λ is to view it as a dimensionless parameter measuring the coupling strength for a hole of given energy ϵ_i and momentum $\mathbf{k}$.

$$\lambda(\epsilon_\mathrm{i}, \mathbf{k}) = \int_0^{\omega_{\max}} \frac{\alpha^2F^{\mathrm{E}}(\epsilon_\mathrm{i}, \mathbf{k}; \omega) + \alpha^2F^{\mathrm{A}}(\epsilon_\mathrm{i}, \mathbf{k}; \omega)}{\omega}\,\mathrm{d}\omega. \tag{4}$$

Here, $\omega_{\max}$ is the maximum phonon frequency.

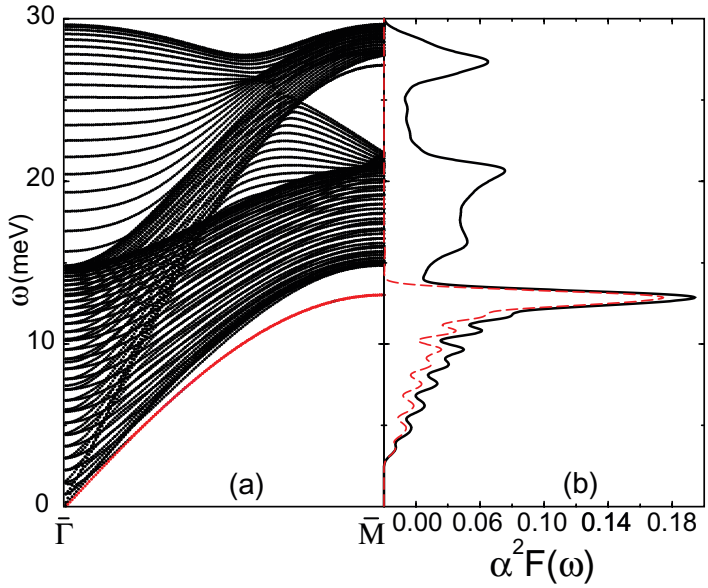

Figure 3. Example of a calculated Eliashberg function. (a) The phonon dispersion from a 31-layer slab calculation in the $\bar{\Gamma}\bar{M}$-direction of the surface Brillouin zone of Cu(111). The Rayleigh mode is marked in red. (b) The Eliashberg function of the hole state at the $\bar{\Gamma}$ point (solid line) and the contribution from the Rayleigh mode to the Eliashberg function (dashed red line). From [34].

Very often the energy change of the scattered electron due to the absorption or emission of a phonon is neglected because the phonon energies are much smaller than the electronic energy scale. While the typical phonon energy lies in the range of meV, the energies of electrons are of the order of eV. Thus, e–ph scattering changes mainly the direction of the electron motion (momentum), while the energy change is negligible. Therefore, one can assume that the initial and final electron energies coincide:

$$\delta(\epsilon_\mathrm{i} - \epsilon_\mathrm{f} \mp \omega_{\mathbf{q},\nu}) \approx \delta(\epsilon_\mathrm{i} - \epsilon_\mathrm{f}). \tag{5}$$

When this so-called quasielastic assumption is applied, the state-dependent Eliashberg function and e–ph coupling parameter are

$$\alpha^2 F(\epsilon_\mathrm{i}, \mathbf{k}; \omega) = \sum_{\mathbf{q},\nu,\mathrm{f}} \delta(\epsilon_\mathrm{i} - \epsilon_\mathrm{f}) |\mathrm{g}^{\mathrm{i,f}}(\mathbf{k}, \mathbf{q}, \nu)|^2 \delta(\omega - \omega_{\mathbf{q},\nu}) \tag{6}$$

and

$$\lambda(\epsilon_\mathrm{i}, \mathbf{k}) = 2 \int_0^{\omega_\mathrm{max}} \frac{\alpha^2 F(\epsilon_\mathrm{i}, \mathbf{k}; \omega)}{\omega} \mathrm{d}\omega. \tag{7}$$

This approximation allows us to use the same Eliashberg function for both emission and absorption processes.

One can average $\alpha^2 F(\epsilon_\mathrm{i}, \mathbf{k}; \omega)$ over electron momentum $\mathbf{k}$ to obtain the energy-resolved spectral function. The latter is defined by the sum over all possible initial electron states with the same energy [2]. In particular, when the energies of initial and final electronic states coincide with the Fermi energy ($\epsilon_\mathrm{i} = \epsilon_\mathrm{f} = E_\mathrm{F}$), we obtain the spectral function and the e–ph coupling

parameter λ (following (7)) as the Fermi surface-averaged quantities:

$$\alpha^2F(E_F;\omega) = \frac{1}{N(E_F)}\sum_{\mathbf{q},\nu}\delta(\omega-\omega_{\mathbf{q},\nu})\sum_{\mathbf{k},i,f}|g^{i,f}(\mathbf{k},\mathbf{q},\nu)|^2\delta(\epsilon_i-E_F)\delta(\epsilon_f-E_F). \tag{8}$$

Here $N(E_F)$ is the electron DOS per atom and per spin at E_F.

The e–ph interaction introduces a shift in the dispersion of electronic states and changes their lifetime. The phonon-induced lifetime broadening of a hole (electron) state can be obtained from the imaginary part of the e–ph self-energy, Σ'', while the real part, Σ', allows us to evaluate the shift in electronic energies. Both parts of the complex e–ph self-energy are fully determined by the Eliashberg function. The imaginary part of the e–ph self-energy is related to the Eliashberg function through the integral over all the scattering events that conserve energy and momentum [44]:

$$\begin{aligned}\Gamma_{e\text{–}ph}(\epsilon_i,\mathbf{k},T) &= 2\Sigma''(\epsilon_i,\mathbf{k};T)\\ &= 2\pi\int_0^{\omega_{max}}\{\alpha^2F^E(\epsilon_i,\mathbf{k};\omega)[1+n(\omega)-f(\epsilon_i-\omega)]\\ &\quad+\alpha^2F^A(\epsilon_i,\mathbf{k};\omega)[n(\omega)+f(\epsilon_i+\omega)]\}\,d\omega.\end{aligned} \tag{9}$$

Here, f and n are the Fermi and Bose distribution functions, respectively. Note that the temperature dependence of $\Gamma_{e\text{–}ph}$ is introduced exclusively by the Fermi and Bose distribution functions. The term in the first square bracket represents the phonon emission and the term in the second square bracket is associated with phonon absorption processes.

In the quasielastic approximation, the contribution of phonons to a hole (electron) state linewidth is written as [44]:

$$\begin{aligned}\Gamma_{e\text{–}ph}(\epsilon_i,\mathbf{k},T) &= 2\Sigma''(\epsilon_i,\mathbf{k};T)\\ &= 2\pi\int_0^{\omega_{max}}\alpha^2F(\epsilon_i,\mathbf{k};\omega)[1-f(\epsilon_i-\omega)+f(\epsilon_i+\omega)+2n(\omega)]\,d\omega.\end{aligned} \tag{10}$$

Let us obtain the behavior of the e–ph linewidth in the limiting cases, $T\to 0$ and $T\gg\omega_{max}$. Note that at $T\to 0$, the Bose distribution function $n(\omega)\to 0$. Then, in the quasielastic approximation, we have

$$T\to 0,\ \Gamma_{e\text{–}ph}(\epsilon_i,\mathbf{k}) = 2\pi\int_0^{\omega_{max}}\alpha^2F(\epsilon_i,\mathbf{k};\omega)\,d\omega. \tag{11}$$

At $T=0$, only phonon emission occurs. Since no electrons can scatter into a hole at the Fermi level, the linewidth for holes at E_F is equal to zero. Then, $\Gamma_{e\text{–}ph}(\epsilon_i,\mathbf{k})$ increases monotonically up to a maximum value at $\omega=\omega_D$ (the maximum phonon energy) as more and more phonon modes become available (see the inset in figure 1(a)). As the temperature increases, the linewidth increases for all electronic energies. This temperature dependence of the linewidth has often been used to extract the e–ph coupling parameter λ for electronic states with energies much larger than the maximum phonon energy.

At elevated temperatures, when k_BT is higher than the maximum phonon energy, the T-dependence of $\Gamma_{e\text{–}ph}(\epsilon_i,\mathbf{k})$ becomes linear with a slope determined by the e–ph coupling parameter λ [44]:

$$\Gamma_{e\text{–}ph}(\epsilon_i,\mathbf{k}) = 2\pi\lambda(\epsilon_i,\mathbf{k})k_BT \tag{12}$$

and λ can be derived from measurements of the lifetime broadening as a function of temperature.

The real part of the self-energy, Σ', allows us to evaluate the renormalization of the electronic energy bands due to the interaction with the phonons (figure 1(a)). One can obtain the renormalized band dispersion, $E(\mathbf{k})$:

$$E(\mathbf{k}) = \epsilon(\mathbf{k}) + \Sigma'(\mathbf{k}, E). \tag{13}$$

Here, $\epsilon(\mathbf{k})$ is the bare dispersion without e–ph coupling and $\Sigma'(\mathbf{k}, E)$ is the real part of the self-energy:

$$\Sigma'(E, T) = \int_{-\infty}^{\infty} \mathrm{d}\nu \int_{0}^{\omega_{\max}} \mathrm{d}\omega' \alpha^2 F(E, \omega') \frac{2\omega'}{\nu^2 - \omega'^2} f(\nu + E). \tag{14}$$

The technique commonly used to determine the mass enhancement factor λ at the Fermi energy is to evaluate the slope of the Σ' at E_{F} because of the identity between the partial derivative of Σ' at the Fermi energy and $\lambda(E_{\mathrm{F}})$:

$$\lambda = \frac{\partial \Sigma'}{\partial E}|_{E_{\mathrm{F}}, T=0\,\mathrm{K}}. \tag{15}$$

The theoretical evaluation of the e–ph interaction generally requires the knowledge of the low-energy electronic excitation spectrum, the complete vibrational spectrum, and the self-consistent response of the electronic system to lattice vibrations. A model approach for evaluating the e–ph interaction in surface states has been proposed in [33, 34, 49]. The model combines three independent approximations: (i) one-electron wavefunctions and energies are calculated with a 1D potential [21, 22]; (ii) phonon frequencies and polarizations are obtained either from one-parameter force-constant model [28] or from an embedded atom model [13]; (iii) the gradient of the one-electron potential is represented by the Ashcroft pseudopotential [5] screened within the Thomas–Fermi approximation. A restriction of this model is that it can only be applied to $s - p_z$ surface electronic states on simple and noble metal surfaces.

All quantities that determine the e–ph coupling can also be obtained from *ab initio* calculations. An advantage of this approach is that all the three ingredients of the e–ph coupling matrix are precisely evaluated on the same footing irrespective of the surface state symmetry. First attempts to evaluate λ focused on calculating only the electronic contribution, while phonon frequencies and polarization vectors were either taken from experimental data or calculated using empirical force constant model. As for the self-consistent adjustment of the one-electron potential to the phonon distortion, it was approximated by neglecting changes in the potential everywhere except within the atomic sphere of the displaced atom [44]. These non-self-consistent calculations appeared to be adequate for many transition metals. However, these approximations are not justified in general, especially for anisotropic or low-DOS materials, as was shown by Winter [118] using linear-response theory for the screening.

Accurate phonon frequencies and polarization vectors, as well as the self-consistent screening can be calculated within the frozen-phonon approach using supercells. In this case, the phonons and electrons are treated with the same total energy formalism and the e–ph coupling is evaluated without any approximation of the crystal potential, which is allowed to adjust self-consistently to the phonon distortion [23, 25, 79]. A good estimation of the average coupling strength λ requires a large number of phonon vectors $\mathbf{q}$ sampled in the Brillouin zone. In the frozen-phonon approach, however, only phonon wavevectors that are commensurate with the lattice and that correspond to reasonably sized supercells can be considered. That makes it difficult to evaluate accurately the average values such as the coupling strength λ, the phonon DOS $F(\omega)$, and the e–ph spectral function $\alpha^2 F(\omega)$. Another technique that can

be employed for calculating the self-consistent change in the potential is the perturbative approach [27] applicable for any **q**. But the perturbative approach has several drawbacks: (i) the slowly convergence of the sum over excited states requires their preliminary calculation by diagonalizing matrices of very large dimension and (ii) the self-consistency realized in this method by inverting the dielectric matrix of the crystal is a rather time-consuming problem.

To date, the most efficient method for calculating lattice dynamical properties of solids is linear-response technique based on the solid-state Sternheimer theory [10, 121]. In this approach atomic displacements are treated as perturbations and the electronic response to the perturbation is calculated self-consistently. This technique has been shown to be particularly efficient because it is not limited to commensurate phonon wave vectors **q**. Moreover, it does not require the knowledge of all unperturbed electronic states as the perturbative approach. It has been implemented with different basis sets for representing electronic wave functions [80, 101].

3. Experimental determination of the e–ph coupling strength

ARPES is a unique experimental tool providing direct access to band structure and many-body effects in solids in general and to the e–ph interaction in particular. It is a firmly established experimental technique and many reviews are available, describing both its theoretical and experimental fundamentals (see for example [29, 60, 63, 65, 71, 85]).

In the following, we focus on the essential points for the study of e–ph coupling in surfaces states. We are mainly concerned with ARPES from nearly 2D states using a spectrometer with infinitely high energy and k-resolution. We also note that the photoelectron wavevector parallel to the surface $\vec{k}_{\parallel}$ is conserved in the photoemission process and as we only treat quasi-2D states, this 2D wavevector is the only one of interest here. For brevity, we denote it as $\vec{k}$.

In this case, and under certain additional assumptions, the photoemission intensity is proportional to the hole spectral function of the sample times the Fermi distribution. The spectral function $\mathcal{A}$, in turn, is used to describe the electronic structure of a solid in the presence of many-body effects. $\mathcal{A}$ can be viewed as the probability of finding an electron with energy $\hbar\omega$ and momentum $\vec{k}$ at a given temperature T. The spectral function is determined by the unrenormalized dispersion $\epsilon(\vec{k})$ and the self-energy Σ. It is usually assumed that Σ is independent of $\vec{k}$. Then $\mathcal{A}$ has the form

$$\mathcal{A}(\omega, \vec{k}, T) = \frac{\pi^{-1}|\Sigma''(\omega, T)|}{[\hbar\omega - \epsilon(\vec{k}) - \Sigma'(\omega, T)]^2 + \Sigma''(\omega, T)^2}. \tag{16}$$

A plot of a typical spectral function for the case of strong e–ph coupling is given in figure 1(b). Under the given assumption that $\mathcal{A}(\omega, \vec{k}, T)$ is proportional to the photoemission intensity, and taking into account that the measured kinetic energy of the photoelectron E_{kin} is merely the binding energy shifted by photon energy and work function, the remaining task is to extract Σ from the measured $\mathcal{A}(\omega, \vec{k}, T)$ and hereby gain the desired information about the e–ph coupling strength.

The methods that have been applied to extract the self-energy from photoemission data are closely related to the traditional measuring modes of ARPES, energy distribution curves (EDCs) and momentum distribution curves (MDCs). An EDC is the photoemission intensity as a function of kinetic energy for a fixed photon energy and a fixed emission angle. An MDC on the other hand is the photoemission intensity as a function of $\vec{k}$ at constant photon and kinetic energies. It is tempting to directly relate EDCs to energy profiles of the spectral function. We

have to bear in mind, however, that an EDC is taken at a constant emission angle, which in general means that $\vec{k}$ is not constant over the EDC energy range. As a consequence, an EDC generally corresponds to a fairly complicated cut through the spectral function. However, under certain conditions, for example for normal emission or for a very small energy range, an EDC is taken at approximately constant $\vec{k}$. In addition, in a modern ARPES set-up, the photoemission intensity can be measured for so many values $(\omega, \vec{k})$ that any cut through the spectral function can be extracted.

Even when care has been taken to account for the energy dependence of $\vec{k}$ in the experiment, it is not straightforward to compare an EDC to an energy profile calculated from (16). Such a profile has a fairly complicated form as a consequence of the energy-dependence of Σ. The expression is simplified considerably, when we assume that $\Sigma'(\omega, T) = 0$ and that $\Sigma''(\omega, T)$ does not depend on ω. We can see from the inset in figure 1 that these conditions are fulfilled in the case of e–ph interaction for peaks with a sufficiently large binding energy. With these assumptions we obtain

$$\mathcal{A}(\omega, \vec{k}, T) = \frac{\pi^{-1}|\Sigma''(T)|}{[\hbar\omega - \epsilon(\vec{k})]^2 + \Sigma''(T)^2}, \tag{17}$$

which is a Lorentzian with the maximum at $\epsilon(\vec{k})$ and a full-width at half-maximum (FWHM) of $2|\Sigma''(T)|$. However, care is necessary when an EDC linewidth is identified with $2|\Sigma''(T)|$ because of the above-mentioned problem that an EDC is strictly measured at a constant emission angle, not at a constant $\vec{k}$ [46, 73, 109]. Furthermore, this approach cannot be applied close to the Fermi energy, the range that is most relevant for transport properties.

The photoemission intensity in the low binding energy regime is more aptly analyzed in terms of MDCs because these are readily represented by (16). The maximum of an MDC is reached when $\hbar\omega - \epsilon(\vec{k}) - \Sigma'(\omega, T) = 0$, and the renormalized and bare-particle dispersions are related according to (13). The expression for the spectral function, equation (16), takes on a particularly simple form in the case of a linear dispersion. We consider only one direction in $\vec{k}$ space and write $\epsilon(k) = vk$ such that the origin of the co-ordinates is at the Fermi level crossing. Then it is easy to show that (16) is a Lorentzian line in $\vec{k}$ for a given ω with the maximum at

$$k_{\max} = (1/v)(\hbar\omega - \Sigma'(\omega)) \tag{18}$$

and

$$\text{FWHM} = 2|\Sigma''(\omega)/v|. \tag{19}$$

In short, $\Sigma''(\omega)$ can be related to the MDC width and, in the case of strong renormalization, $\Sigma'(\omega)$ can be related to the MDC maximum. We note, however, that either approach relies on knowing the unrenormalized dispersion $\epsilon(\vec{k})$. The key problem is that this dispersion is not known. This is a familiar situation for high temperature superconductors for which a strong band renormalization is found. Different solutions have been employed to solve this problem. One is to extrapolate $\epsilon(\vec{k})$ from states at higher binding energy where the renormalization is negligible [114]. Another is to take $\epsilon(\vec{k})$ from a calculation of the band structure, which does not incorporate the many body effects. A third is to obtain $\epsilon(\vec{k})$ from a measurement of the dispersion at elevated temperatures where the renormalization due to e–ph coupling is negligible [65]. Finally, $\epsilon(\vec{k})$ and the self-energy can be determined by a self-consistent fitting procedure [68]. The latter approach relies on the fact that for a given $\epsilon(\vec{k})$, Σ' and Σ'' can be evaluated and subsequently compared using the Kramers–Kronig transformation.

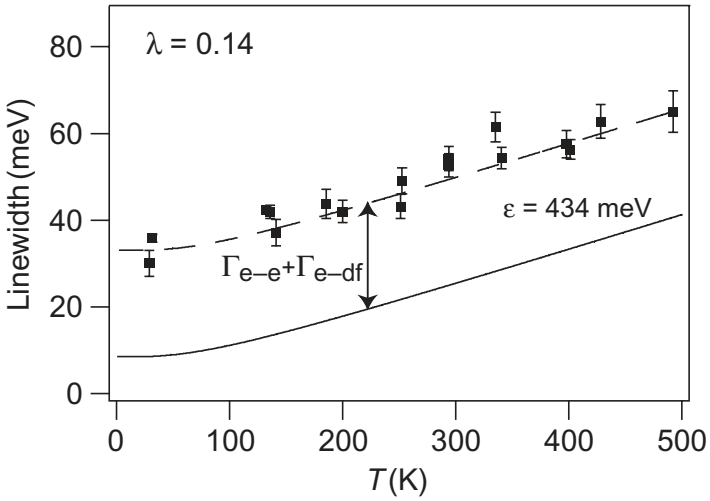

Figure 4. Temperature-dependent linewidth of the Cu(111) surface state at $\bar{\Gamma}$. Data points are taken from [87]. The solid line is the e–ph contribution to the linewidth calculated within a 3D Debye model and assuming $\lambda = 0.14$. The dashed line is a rigid displacement of the solid line in order to take e–e and e–df scattering into account.

A finite experimental energy resolution gives rise to a further complication when we try to extract the self-energy from photoemission data close to the Fermi energy. A non-negligible resolution affects the measured dispersion such that k_F is shifted towards the direction of occupied states [65]. k_F does therefore not coincide with the observed MDC maximum at E_F, even though any renormalization vanishes at the Fermi energy. Even if we knew $\epsilon(\vec{k})$, Σ' could therefore only be determined reliably close to the Fermi energy, if the resolution were either negligible or properly accounted for.

We see that under certain conditions it is possible to determine the real or imaginary part of the self-energy from the spectral function measured by ARPES. The next task in the analysis is to relate this to the e–ph coupling strength. The most fundamental quantity for describing the e–ph interaction is the Eliashberg function $\alpha^2 F$, which cannot directly be extracted from the experiment. It is, however, closely related to the Σ through equations (10) and (14). The difficulty is that there is no trivial inversion to these equations and that the e–ph coupling effects in Σ are temperature-dependent, whereas $\alpha^2 F$ is not. In the following, we briefly discuss and illustrate different approaches that have been proposed to extract information about the e–ph coupling from photoemission data.

A simple approach that is used frequently (for example see [8, 9, 42, 56, 64, 74, 86, 87, 93, 111]) is to measure the temperature-dependent EDC linewidth of a state far away from E_F. In this case, we have seen from (17) that the linewidth is $2|\Sigma''(T)|$. Figure 4 shows the linewidth of the Cu(111) surface state at the $\bar{\Gamma}$ point at a binding energy of 434 meV, as well as a calculation for the expected Γ_{e-ph} from (10), using a value of $\lambda = 0.14$. The data points are taken from the work by McDougall *et al* [87]. Evidently, the agreement between the calculation and the data points is very good if the latter are rigidly shifted to higher energy. This is expected according to (1) because the measured linewidth does not only contain the e–ph contribution but also the e–e and e–df contributions, which are assumed to be independent

of temperature. In their original paper, McDougall *et al* fitted the data points with a line, i.e. using (12) plus an offset, rather than the full expression given in (10). While this simplification is formally only justified for temperatures much higher than the Debye temperature Θ_D (343 K for Cu), it is, in practice, already quite useful for temperatures similar to Θ_D, as evident from the figure.

If the (surface) Debye temperature is too high for (12) to be a good approximation, this simple approach of data analysis becomes problematic. In order to extract information about the e–ph coupling from temperature-dependent data, it is then necessary to use (9) but this requires a model for the Eliashberg function α^2F. Frequently one employs a simple model for α^2F, such as the 3D Debye model with

$$\alpha^2F(\omega) = \lambda\left(\frac{\omega}{\omega_D}\right)^2, \quad \omega < \omega_D \tag{20}$$

and

$$\alpha^2F(\omega) = 0, \quad \omega > \omega_D,$$

which has also been used to calculate the solid curve in figure 4. Alternative models are an Einstein model or a 2D Debye model [30, 49]. Unfortunately, this introduces a certain degree of arbitrariness and it requires the precise knowledge of the surface Debye temperature.

In addition to the method that relies on the EDC linewidth and (17), several other approaches were introduced to obtain the self-energy from the renormalized dispersion. A good illustration of the different possibilities is given in figure 5, which shows surface state dispersion for a Mo(110) surface state, the imaginary part of the self-energy and the real part of the e–ph self-energy. The dispersion, as determined from MDCs, shows a clear kink close to the E_F which is caused by e–ph coupling. Σ' was determined according to (13) from these data and the dispersion interpolated from higher binding energies, assuming that the position of the Fermi level crossing is not affected by the e–ph interaction.

The figure also shows the Σ'' that was determined from the EDC peak width, an approach that only works if the coupling is not too strong and the Fermi cut-off is taken into account. Close to E_F, Σ'' shows the typical signature of e–ph coupling with a strong change in a small energy window, which is schematically shown in figure 1. The dashed line shows a model calculation for the e–ph part of Σ'' and the dotted line shows the Kramers–Kronig transformation of this, which is in good agreement with Σ'. The calculated Σ'' that stems from a calculated bulk α^2F and (9) agrees well with the data; and the surface Debye temperature is similar to the bulk value, suggesting a similar mass enhancement parameter λ. Interestingly, the measured Σ'' shows an increase at higher binding energies which cannot be accounted for by e–ph interaction. This is ascribed to e–e interaction. Σ'' is also 26 meV higher than the calculated value, which is ascribed to e–df scattering.

Figure 6 illustrates the case of stronger coupling that is found on the Be(0001) surface. Apart from the strong coupling, beryllium is a favorable material for the observation of e–ph coupling because of the high phonon energies and Debye temperature, which permit detailed observation of the effect without the need of an exceedingly high energy resolution. Figure 6 shows low-temperature high-resolution data from the work of Hengsberger *et al* [50, 51]. EDCs from the Be(0001) surface are given as the dispersion approaches E_F. Near the Fermi level crossing the EDCs clearly deviate from the Lorentzian lineshape (17) because both conditions for the validity of this equation ($\Sigma'(\omega, T) = 0$ and $\Sigma''(\omega, T) = \text{const.}$) are violated. This

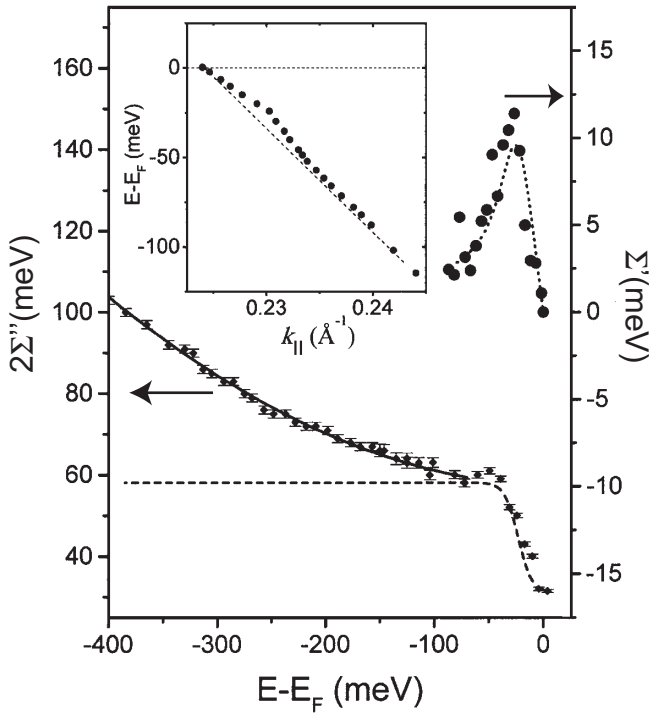

Figure 5. E–ph measured data for a Mo(110) surface state after Valla *et al* [114]. Σ' and Σ'' are plotted as a function of binding energy. Σ'' was obtained from the width of the quasiparticle peak. The dashed (dotted) line shows the calculated e–ph contribution to Σ'' (Σ'). The dashed line is shifted up by 26 meV. The inset shows the renormalized (points) and bare dispersion (dashed line) used to extract Σ'.

complicated lineshape is a direct confirmation of an old prediction [36]. In this case, a simple analysis of temperature-dependent data to extract information about e–ph interaction would clearly be aggravated by the complicated lineshape.

Instead, figures 6(b) and (c) show the determination of Σ' and how information about λ is extracted from more recent data [17]. The renormalized dispersion $E(k)$ is represented by the solid line that tracks the maxima of the MDCs, according to (16). The bare dispersion $\epsilon(k)$ is found from two conditions: (i) it has to cross E_F at the same k_F unless there is a significant distortion of the band by a finite energy resolution and (ii) it must coincide with $E(k)$ for high binding energies as $\Sigma'(\omega)$ approaches 0. In the present case, $\epsilon(k)$ is described by a second-order polynomial. The resulting self-energy $\Sigma'(E)$ can now be determined using (13). Alternatively, $\Sigma'(\epsilon)$ could be determined from a fit to the width of the state, as in figure 5 but the position of a peak is generally more stable in noisy data than its width.

The resulting $\Sigma'(E)$ is given in figure 6(c). From this it is possible to extract λ in several ways. The simplest is to use (15) and to extract λ from the slope of Σ' near E_F. This is illustrated by the short bold line near E_F, which corresponds to a $\lambda = 0.9$. It is crucial to keep in mind the conditions for this approach to be valid: the temperature must be very low compared to Θ_D (fulfilled for Be) and the energy range used must be very small because only the slope *at the Fermi energy* is of interest.

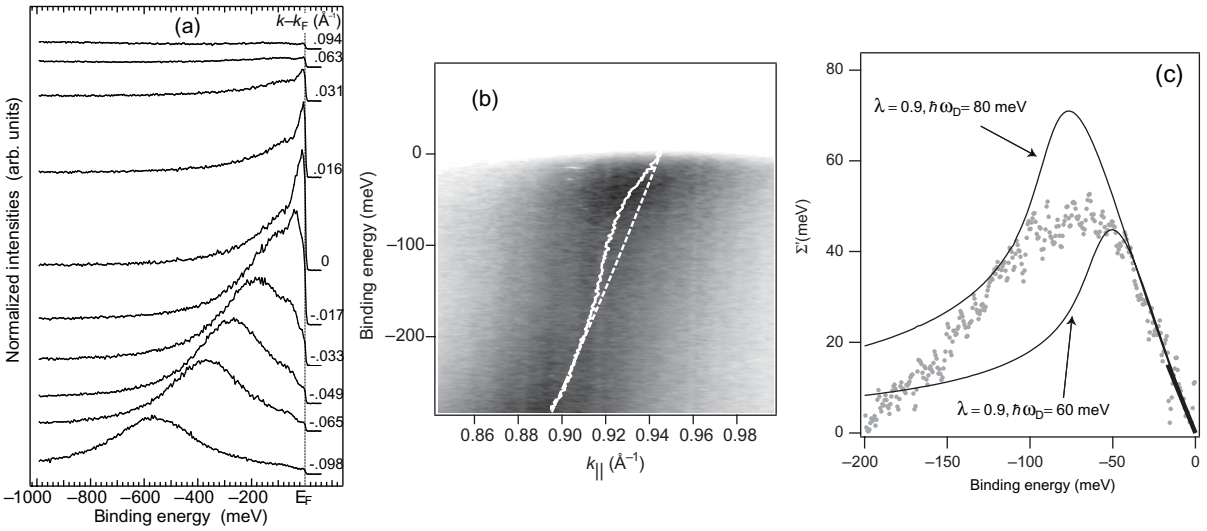

Figure 6. (a) High-resolution photoemission spectra of the Be(0001) surface state near k_F at $T = 12$ K. From [51]. (b) Photoemission intensity of the same state near E_F at $T = 70$ K. The dashed line shows the bare dispersion $\epsilon(k)$ and the solid line tracks the MDC maxima, giving the renormalized dispersion $E(k)$. (c) Resulting Σ'. The different lines are models to extract λ as described in the text. From [39].

Alternatively, the entire Σ' can be fitted with a model self-energy, for example using a Debye model (20) to calculate α^2F and then (14) to calculate Σ'. In the Debye model, this calculation contains two parameters λ and ω_D as well as the sample temperature. Two such calculations are shown in figure 6(c) for $\lambda = 0.9$ and $\hbar\omega_D = 80$ meV as well as for $\lambda = 0.9$ and $\hbar\omega_D = 60$ meV. Roughly spoken, and at low temperature, λ gives the slope of the curve at E_F and ω_D determines the maximum of the curve. In the present case, it is evident that the Debye model is too simple to account for the detailed shape of Σ'. No set of parameters can be found, which results in a satisfactory overall fit.

Recently, a different approach to e–ph data analysis has been proposed, which potentially solves several of the problems mentioned above. The experimentally determined self-energy Σ' or Σ'' is not analyzed using a model for α^2F combined with (14) or (10). Rather, $\alpha^2F(\omega)$ is directly obtained from Σ' using an integral inversion of (14) based on a maximum entropy approach [104, 112]. This method directly yields $\alpha^2F(\omega)$, i.e. the most fundamental property for the description of e–ph interaction, and it has the potential to provide interesting fine structure in this function. For its reliable application very high quality data are needed.

4. Some examples

In this section, we present some results for the e–ph coupling at surfaces. We mainly discuss simple and noble metal surface states for which both experimental data and *ab initio* calculations are available. For noble metal surfaces, we also include a brief discussion of the e–ph interaction in image potential states. In the end of the section, we also present a few other examples, such as the e–ph coupling in semimetals, adsorbate systems, quantum wells and free-standing monolayers (MLs).

Table 1. E–ph coupling parameter λ and linewidth (in meV) for surface electronic states.

	E (eV)	λ calc.	λ expt.	Γ_{e-ph} $T = 0$ K	$\Gamma_{Expt.}$
Al(001)					
$\bar{\Gamma}$	−2.8 [94]	0.51 [106]	Consistent w. 0.51 [62]	35 [106]	267 [62]
		0.23 [33]		18 [33]	
				26 [90]	
$\bar{X}$	−4.55 [78]	0.78 [106]		50 [106]	
Be(0001)					
$\bar{\Gamma}$	−2.78 [11]	0.38 [32]	1.15 [9]		281 [105]
			0.87 [73]		
Mg(0001)					
$\bar{\Gamma}$	−1.63 [103]	0.28 [77]	0.27 [64]	19 [77]	133 [64]
$\bar{M}$	−0.95 [103]	0.38 [77]		20 [77]	
Ag(111)					
$\bar{\Gamma}$	−0.04 [61]	0.12 [33]	0.12 [34]	3.7 [33]	6 [67]
				7.2 [67]	6 ± 0.5 [96]
Cu(111)					
$\bar{\Gamma}$	−0.4 [41]	0.16 [33]	0.14 ± 0.02 [87]	7.3 [33]	24 [67]
			0.11 [34]	21.7 [67]	23 ± 1 [96]
				5.67 [90]	
Au(111)					
$\bar{\Gamma}$	−0.5 [47]	0.11 [33]	0.34 ± 0.01 [74]	3.6 [33]	18 [67]
			consistent w. 0.11 [62]	18.9 [67]	21 ± 1 [96]

An overview of both experimental and theoretical results for simple and noble metals is given in table 1. Comparing the calculated and experimentally determined mass enhancement parameters λ shows a very satisfactory agreement for this class of materials. Details of experiments and calculations are discussed in the following.

4.1. Noble metal surfaces

The (111) surfaces of the noble metals Ag, Cu and Au all support a similar Shokley-type surface state in the bulk L-gap of the metal. This surface state has long been an important model system for the study of electronic structure and lineshapes by ARPES (see [96] for recent high-resolution data as well as for a historic overview of the field). The surface state is well-localized within a few layers of the surface and has a small binding energy such that the e–ph interaction for these states should be strongly influenced by surface phonon modes. The e–ph coupling turns out to be very similar for all three surfaces.

Results of a theoretical investigation of the phonon-mediated decay of surface states on Ag(111), Cu(111) and Au(111) were presented in [33, 34, 115]. The electronic states were defined using model potentials [20, 22], which reproduce the correct surface projected band gap at the $\bar{\Gamma}$ point and the surface state energies for the systems. The phonon modes were obtained from a single force constant model, where the force constant was fitted to reproduce the elastic constants and the maximum bulk phonon energy.

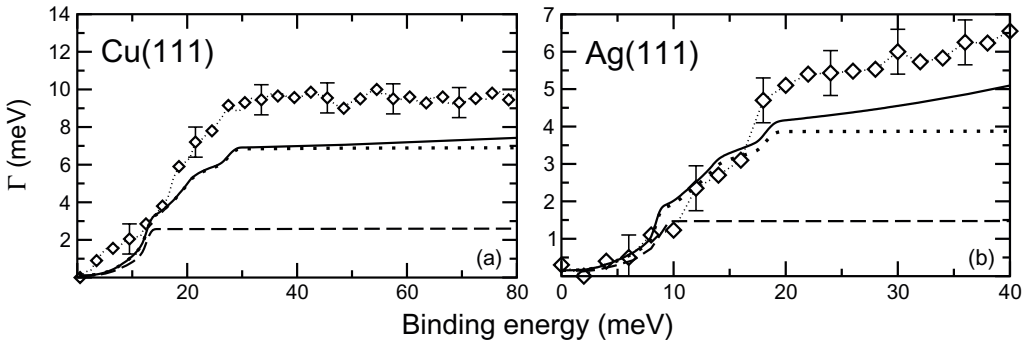

Figure 7. (a) Lifetime broadening of the Cu(111) surface hole state as a function of binding energy, $\Gamma_{e-e} + \Gamma_{e-ph}$ (solid line), Γ_{e-ph} (dotted line), Rayleigh mode contribution to Γ_{e-ph} (dashed line) and photoemission data (diamonds). (b) The same as in (a) for Ag(111). Figure after [34].

Figure 7 shows the result of such a calculation for Cu(111) and Ag(111) and the comparison to experimental data, obtained from the linewidth of the state near E_F [34]. The overall agreement between calculation and experiment is very good. As expected because of the small penetration and as shown in figure 3, the Rayleigh mode gives a very significant contribution to $\alpha^2 F$ and hence to Γ_{e-ph} for these surfaces. It is the dominant mechanism for hole decay at small energies for which e–e scattering is insignificant. Note also that Γ_{e-ph}, or equivalently Σ'', which results from this calculation shows considerable fine structure.

Another important result from the calculations is that the coupling strength λ is relatively independent of the binding energy of the hole. Again, this is in good agreement with experimental data that does not point towards any strong binding energy dependence of λ [34, 74, 87].

It should be mentioned that an initial experimental study of the e–ph coupling on Au(111) gave a value of $\lambda = 0.33$ in rather poor agreement with the calculated $\lambda = 0.11$ [33]. Later this discrepancy was ascribed to the thermal excitation of defects at elevated temperature and the experimental linewidth could be reconciled with $\lambda = 0.11$ [62]. This effect is discussed in more detail in connection with e–ph interaction on Al(001) below.

The e–ph contribution to the lifetime broadening of image-potential states and the respective e–ph coupling parameter λ were calculated for Ag(100) and Cu(100) [31]. It was shown that the e–ph coupling in the first image-potential state on these surfaces is very weak, $\lambda \sim 0.01$, and Γ_{e-ph} amounts to only 1–5% of the total lifetime broadening value Γ. This weak e–ph interaction was explained by a small penetration of the image-potential states into the bulk [91, 100]. It was also found that both surface and bulk phonon modes are important to correctly describe the phonon-mediated decay of image-potential states.

4.2. Be(0001)

The Be(0001) surface is a nearly ideal system to test the e–ph coupling of surfaces because the $\bar{\Gamma}$ surface state resides in a wide gap and contributes significantly to the total DOS at the Fermi level. In fact, the bulk DOS of Be is not free-electron like due to the strongly covalent bonding character in this metal but the surface DOS is, justifying the view of the surface state as a 2D free electron gas which is de-coupled from the bulk [95].

Several experimental studies and one *ab initio* calculation of the e–ph coupling on Be(0001) have been published [9, 32, 50, 51, 73, 112]. The experimental values of λ spread over an unsatisfactory large range between 0.7 and 1.18, even though some care has to be exercised here because the lowest reported value by Tang *et al* might have been caused by oxygen contamination of the sample [17] and not all values have been measured at E_F or at the same direction of $\vec{k}_F$. The theoretical value of λ at E_F was found to be 0.9, in good agreement with the available data. In any event, the coupling is much stronger than in bulk Be for which $\lambda = 0.21$–0.23 (theory [88, 107]).

4.3. Mg(0001) and Al(001)

The $\bar{\Gamma}$ surface states of Mg(0001) and Al(001) have a rather different character from those of the noble metal (111) surfaces and of Be(0001). Both reside in a narrow projected band gap and penetrate deeply into the bulk. Thus, one would expect a certain similarity to actual bulk states, both in their electronic character and in their e–ph interaction.

An *ab initio* study of the e–ph coupling and its contribution to the lifetime broadening of the $\bar{\Gamma}$ surface state on Al(001) was reported in [106]. As expected, the largest contribution to the e–ph coupling comes from the scattering of excited electrons with bulk phonon modes. In general, the surface phonons contribute less than 30% to the e–ph coupling. This fact was also proved by model potential calculations [33], where it was shown that the interband scattering in the $\bar{\Gamma}$ surface state gives the most important contribution to the Eliashberg function.

Another important finding was that the low- and middle-energy phonons are more involved in the scattering processes of electrons than the high-energy phonon modes, unlike in the case of bulk Al and other simple metals such as Be and Mg, where the lower-energy part of the phonon spectrum is strongly suppressed by e–ph matrix elements [12, 77, 80, 102, 107].

The calculated $\lambda(\bar{\Gamma}) = 0.51 \pm 0.01$ [106] is somewhat higher than the e–ph coupling parameter averaged over momenta both at the Fermi level of bulk Al, $\lambda(E_F) = 0.43$, and at the Fermi energy of the Al(001) surface, $\lambda(E_F) = 0.45$.

The obtained results also showed that both the e–ph coupling and the linewidth of excited electrons experienced rather weak variation with the energy and momentum position of a hole (electron) state in the surface energy band. In particular, the variation range of $\lambda(\epsilon_{\mathbf{k}_i})$ does not exceed 0.1. However, the strength of the e–ph coupling varies strongly from one surface electronic band to another. For example, for the surface electronic bands at the Brillouin zone boundary the values of $\lambda(\epsilon_{\mathbf{k}_i})$ are twice as large than those obtained for excited electrons at the $\bar{\Gamma}$ surface band. On the other hand, the directional anisotropy in the e–ph coupling on Al(001) is very weak.

Experimental results for this surface state at $\bar{\Gamma}$ were presented in [62]. The temperature-dependent linewidth of the state had been measured over a wide temperature range but the data could not be accounted for using (10) or (12) plus a temperature-independent offset. Indeed, a fit to the high temperature part of the data, in the range where (12) should be applicable, resulted in $\lambda = 0.84$, in very poor agreement with the theory. This problem could be resolved by taking into account the possibility of e–df scattering from thermally excited defects. While the e–df scattering strength is still assumed to be temperature-independent, the number of defects is not and there is an exponentially increasing probability of thermally excited defects at elevated temperatures. With this assumption, a satisfactory fit to the data could be obtained, which was consistent with the theoretical value for λ.

At the center of the surface Brillouin zone, $\Gamma_{e-ph}(\bar{\Gamma}) = 35$ mev at $T = 0$ and increases up to 90 meV at room temperature. The calculated e–e contribution $\Gamma_{e-e} = 131$ meV [18] is much bigger than the e–ph part at such excitation energies. However, at room temperature they become comparable. The measured linewidth at $\bar{\Gamma}$ extrapolated to 0 K is 267 meV [62] whereas the calculated e–e and e–ph contributions taken together give only 166 meV. The large difference is attributed to defect scattering.

The e–ph contribution to the linewidth of the surface hole state at $\bar{\Gamma}$ has also been studied using a model calculation [33]. Eiguren *et al* obtained $\lambda(\bar{\Gamma}) \approx 0.23$ and $\Gamma_{e-ph}(\bar{\Gamma}) \approx 18$ meV. Both values are nearly half as large than those reported in [62, 106]. Such a difference can be accounted for by using in the model calculation [33] the gradient of the one-electron potential as the Ashcroft pseudopotential screened within the Thomas–Fermi approximation. This approximation gives an accurate description of electronic structure of bulk Al at the Fermi level but it is less accurate for electronic states far (2–6 eV) below E_F. Thus, the value of λ obtained in the model calculation for this surface state at the Fermi level comes up to 0.55 and $\Gamma_{e-ph}(E_F) \approx 37$ meV [33].

The $\bar{\Gamma}$ surface state on Mg(0001) is similar in character to the one on Al(001) in that it penetrates very deeply into the bulk. The temperature-dependent linewdith of the state has been analyzed along the same lines as discussed above and the results have been interpreted using a 3D Debye model for α^2F. A problem in this interpretation was the unknown surface Debye temperature Θ_D: a good fit to the data could be achieved for a wide range of λ values depending on the choice of Θ_D. This is not surprising: both λ and Θ_D appear in the model α^2F (20) and a change of one value can almost entirely be compensated by a corresponding change in the other. The problem was resolved by defining an effective Θ_D based on experimental data on the surface vibrations combined with a calculated probability density function of the surface state. This resulted in a value of $\lambda = 0.27$.

A detailed *ab initio* study of the e–ph interaction and phonon-mediated contribution to the linewidth of surface electronic states on Mg(0001) was reported in [77]. The results are very similar to those obtained for Al(001): there is a strong interaction of electrons with bulk phonon modes because the surface electronic states in both cases lie very close to bulk electronic bands. λ was found to have a value of 0.28, in excellent agreement with the experimental data.

4.4. Semimetal surfaces

The surfaces of the semimetals Bi and Sb are in sharp contrast to the two above examples because their surface states are placed in wide projected band gaps and their surface electronic structure is very different from that of the bulk. Bulk Bi and Sb are typical for the group V semimetals in having a very low DOS at the Fermi level. The presence of the surface states, however, turns the surfaces into good metals. This has been found for Sb(111) [53, 110] and all Bi surfaces studied so far (Bi(110) [1], Bi(111) [6, 52], Bi(100) [57] and Bi(114) [117], for a review see [55]). The metallic character of the surface is closely related to the strong spin–orbit splitting of the surface state bands [55, 69] and, interestingly, can also be understood based on the similarity of Bi and the $Bi_{0.9}Sb_{0.1}$ alloy which can be classified as a topological insulator and therefore has to support metallic surface or edge states [58, 59, 113]. Bi surfaces therefore provide the opportunity to study the e–ph interaction for a nearly 2D electronic system with strong spin–orbit splitting. The coupling strength near the Fermi level has been studied experimentally for Bi(111) [7, 43] and Bi(110)[65]. For Bi(100) the coupling was studied for a range of different binding energies.

The e–ph coupling close to E_F for the hole pocket near the $\bar{\Gamma}$ point of Bi(111) has been studied by two groups. Ast and Hüochst have analyzed the MDC linewidth as a function of binding energy near E_F [7] and Gayone *et al* have analyzed the temperature dependence of the MDC linewidth of the same state, also near the Fermi level crossing [43]. The resulting values for λ obtained by Ast and Höchst (0.6 or 2.3, depending of the choice of model) and by Gayone *et al* (0.4) are quite different. This apparent contradiction was eventually solved by Kirkegaard *et al* [65]. These authors have shown that the finite spectrometer energy resolution needs to be taken into account in the type of analysis performed by Ast and Höchst. A simple estimate shows that if this is done, the final value of λ is quite close to that obtained by Gayone *et al* [65].

Kirkegaard *et al* have studied the e–ph coupling for two different surface states of Bi(110), the hole pockets near $\bar{\Gamma}$ and $\bar{M}$ [65]. Σ'' was extracted from MDCs, both as a function of temperature and energy. The resulting large and 2D data sets have been fitted to (10) using both the Debye and the Einstein model for the Eliashberg function. Because of the large data set, the problem of determining both λ and the Debye (or Einstein) energy could be solved in a satisfying way. The resulting values of λ turned out to be the same in the Debye and Einstein models, a fact that is not surprising because much of the data was taken at elevated temperatures (relative to the Debye temperature), where the precise nature of the phonon spectrum becomes unimportant (see equation (12)). The λ values obtained from this analysis are 0.19(3) and 0.27(2), near the $\bar{\Gamma}$ and $\bar{M}$ points, respectively.

The e–ph interaction on Bi(100) was determined by Gayone *et al* by studying the EDC linewidth of a surface state as a function of binding energy and temperature [42]. Keeping in mind (17), this approach is only possible for binding energies much larger than a typical phonon energy. For Bi this is not a problem because the maximum phonon energy is very small, only 13.8 meV [120]. The surface state used for the study was the state in the $\bar{\Gamma} - \bar{K}_2$ direction which has two local extrema in the dispersion, a maximum at a binding energy of 330 meV and a minimum at 70 meV [42, 57].

The final result of the analysis is λ as a function of binding energy as shown in figure 8. The energy dependence of λ is very strong; it changes from 0.72 to 0.20 in an energy range of less than 300 meV. From this it is evident that λ determined in this way cannot be interpreted as the mass enhancement parameter at E_F. A spectroscopic interpretation as a parameter measuring the e–ph strength at a certain binding energy and $\vec{k}$ is more appropriate.

The strong energy dependence of λ was essentially explained by the transition from a 3D system at high binding energies (bulk plus surface) to a merely 2D system close to E_F. The Eliashberg function (6) is a sum over the different possibilities to fill a hole state with an electron using a phonon to provide energy and momentum (see figure 2). If we assume that the matrix element for the scattering process is only weakly energy dependent, the change of λ can be understood from simple phase space arguments; at high binding energies there are many bulk states available in which a hole can scatter with the help of a phonon. Close to the Fermi energy the density of bulk states is very small. In order to illustrate the argument, figure 8 also shows a plot of the calculated bulk DOS, scaled in an arbitrary way. For high binding energies, the change in the bulk DOS mimics the change in λ, as expected from the simple argument above. For small binding energies, the bulk DOS essentially vanishes but λ stays finite. The scattering processes leading to e–ph interaction in this energy range are therefore most likely to involve other surface states.

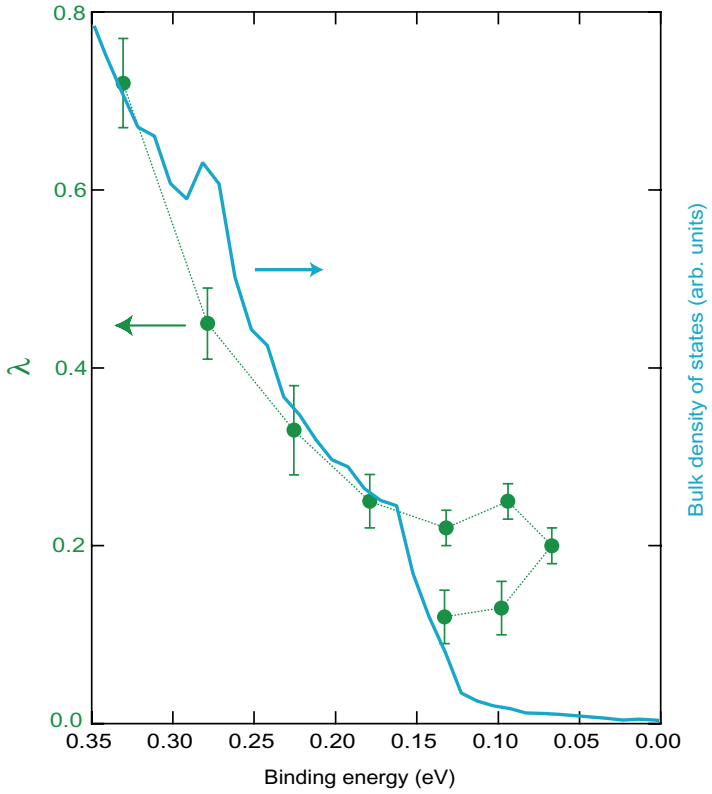

Figure 8. E–ph coupling parameter λ as a function of the binding energy. The dashed line between the data points connects the points as they lie on the $\bar{\Gamma} - \bar{K}_2$ line. Also shown is the bulk density of electronic states in Bi as a function of binding energy as calculated using the tight binding parameters from Liu and Allen [81]. After [42].

4.5. Overlayers and quantum well states (QWSs)

Most of the investigations have been performed for surface states formed on clean metal surfaces while only few have been devoted to the study of an e–ph coupling parameter λ in QWSs formed in ultrathin metal films on metal substrates [15, 16, 24, 35, 38, 48, 49, 83, 84, 89]. In particular, in [37, 38] the calculation results of the e–ph interaction in QWS for an ML of Na on Cu(111) have been presented. As was shown experimentally by using photoemission spectroscopy [15] two-photon photoemission technique [40], and scanning tunneling spectroscopy [66], the $\bar{\Gamma}$ QWS in this system is located just below the Fermi level, E_F. The e–ph interaction in the 1 ML Na/Cu(111) has been calculated by Hellsing *et al* [48] simulating the entire phonon spectrum of the system by a single frequency (Einstein model) that corresponds to vertical vibrations of the rigid Na ML. This may lead to overestimation of λ and Γ_{e-ph} despite the use of an accurate one-electron potential and wavefunction of QWS. Simple estimates of λ and Γ_{e-ph} within 2D and 3D Debye models significantly lowered these quantities [19]. The role of the whole phonon spectrum of 1 ML Na/Cu(111) in the e–ph interaction in QWS of the 1 ML Na/Cu(111) system has been studied by Eremeev *et al* [38], where it was conclude that the role of vertical Na vibrations in λ and Γ_{e-ph} is rather small.

The 1 ML Na/Cu(111) semi-infinite system was simulated using a slab model with 31 atomic layers of Cu(111) and Na atoms located on both sides of the Cu slab. Due to the large number of atoms the following model was used. The model combines three independent approximations to evaluate the e–ph coupling matrix elements: (i) one-electron wave functions and energies are calculated using a 1D potential specially designed for 1 ML Na/Cu(111) [19]; (ii) phonon frequencies and polarizations for 1ML Na/Cu(111) are obtained from an embedded atom model [13]; (iii) a gradient of the one-electron potential is represented by the Ashcroft pseudopotential [5] screened within Thomas–Fermi approximation.

It was shown that the largest contribution to the e–ph coupling comes from the interaction of the QWS with horizontal (in-plane) vibrations of Na atoms and with vertical vibrations of atoms of the top Cu substrate layer. That is very distinct from the results obtained by using the Rayleigh like mode (Einstein mode) to simulate the entire phonon spectrum of 1 ML Na/Cu(111) [15, 48]. The calculation of λ gave $\lambda = 0.14$. This value is close to $\lambda = 0.16$ obtained theoretically [33, 34] and $\lambda = 0.14 \pm 0.02$ deduced from photoemission measurements [85, 87] for the surface state on clean Cu(111). Despite this coincidence it is worthy to note that λ in 1 ML Na/Cu(111) and λ in Cu(111) are formed by different phonon modes (where Cu vertical vibrations (Rayleigh mode) provide 30–35% of the full phonon-induced contribution to the surface state decay rate on Cu(111) [33, 34]), therefore, the coincidence should be considered to a large extent as accidental. Nevertheless, at T=0 K, $\Gamma_{e-ph} = 5.4$meV obtained for 1 ML Na/Cu(111) is smaller than $\Gamma_{e-ph} = 7.3$meV calculated for Cu(111).

In contrast to the work on ultrathin films, a considerable number of studies deal with the effect of increasing film thickness on e–ph coupling in quantum well systems. Luh *et al* have determined the coupling strength as a function of film thickness in the Ag/Fe(100) system [82]. The strength is determined in this case using the temperature dependent linewidth of several QWSs. The experimentally observed enhancement of the coupling with decreasing film thickness is attributed to the increased contribution of the quantum well interface. Later work by the same authors on this system reveals that the e–ph coupling strength differs dramatically between different QWSs [92]. The λ for the sp-band QWS in this system is about 0.5, i.e. 35 times larger than that derived from the d-band states. Mathias *et al* also observe a linearly decreasing coupling strength with increasing film thickness in silver films grown on copper [83]. They, however, find step-like coupling strength *increases* with film thickness that occur when a new higher-order QWS is established.

In the studies of lead films on Si(111) [14, 45, 122] at low temperatures it was shown that the superconducting energy gap and critical temperature T_c that depend on e–ph coupling are closely related to the film thickness. It was also demonstrated that both the transition temperature and the e–ph coupling strength oscillate in phase with the electronic DOS at the Fermi energy as functions of the Pb film thickness.

4.6. H/W(110)

Another system that has been studied extensively with photoemission to reveal the effect of the e–ph interaction on quasi-particle states is hydrogen adsorbed on W(110). Hydrogen adsorption is known to induce surface states at the (110) surface of tungsten, and Rotenberg *et al* have shown that one of these, an elliptical hole pocket around the $\bar{S}$ point, shows significant

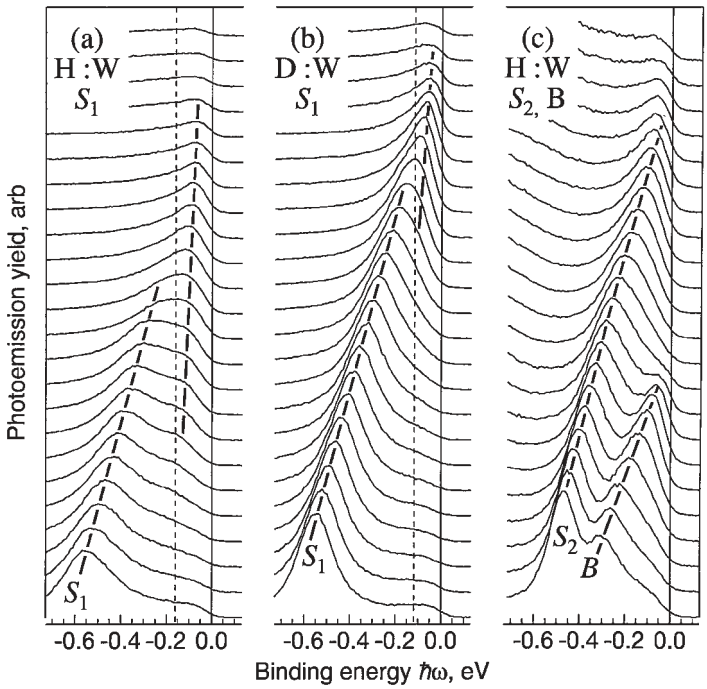

Figure 9. Series of photoemission spectra of H and D covered W(110) from Rotenberg *et al* [99]. Spectra are taken along paths crossing the Fermi contours of state S_1 (a and b), and S_2 and B (c).

renormalization [99]. EDCs are split close to the Fermi energy at an energy scale comparable to an adsorbate vibrational mode, see figure 9(a).

This renormalization can unequivocally be attributed to coupling with adsorbate vibrations by a strong isotope effect. When the surface is covered with deuterium instead of hydrogen, the surface electronic structure is largely unaltered. The energy scale on which the renormalization takes place, however, is significantly reduced, as is indicated by the dotted lines in figure 9. This result agrees well with the expectation that the energy of the involved vibrational mode should be reduced by about $\sqrt{2}$. In addition, as we can see by comparing the spectra in figures 9(a) and (b), the linewidth of the S_1 feature is strongly reduced upon replacing H with D.

Later work by Rotenberg and Kevan shows a more detailed analysis of the H/W(110) system [98], in which the coupling strength λ of the S_1 state is determined at different positions on its Fermi contour. The coupling strength is found to vary between zero and approximately 0.8. The strong variation in coupling strength of the S_1 feature is attributed to variations in the degree of surface localization of the state. The maximum value is a dramatic enhancement in comparison to bulk W, with a λ of 0.2.

A direct evidence of the influence of e–ph coupling on adsorbate phonon mode dispersion and line shape was obtained analyzing changes in broadband reflectivity measurements on W(100)/H and Mo(100)/H as a function of coverage [97].

In summary, this work shows that the use of adsorbates provides us with a promising route to tailor the low energy properties of surfaces, as the e–ph coupling can be tuned by the introduction of particular modes.

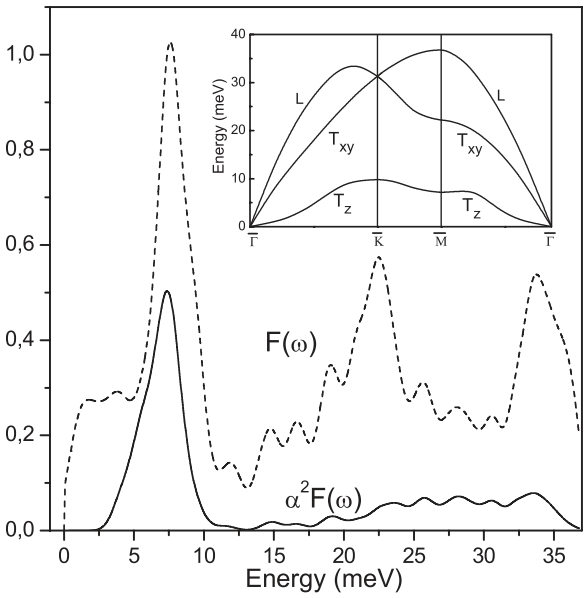

Figure 10. Eliashberg function $\alpha^2 F(\omega)$ averaged over momentum at E_F (solid line) and phonon DOS F(ω) (dashed line) for an ML of Mg(0001). In the inset the phonon spectrum is shown.

4.7. E–ph interaction in free standing monolayers

In the theoretical studies of many metal surfaces [32]–[34], [77], the important role of surface phonon modes in the e–ph coupling was emphasized. These vibrations are often softer than the bulk ones and couple in a very efficient way to electrons, giving a strong contribution to the e–ph scattering. In the limit case of a single layer, the smaller (by 6−9%) value of the optimized lattice parameter [75, 76] results in stronger in-plane atomic interactions and, as a consequence, a higher maximum phonon frequency compared to the bulk or surface value. However, unlike the in-plane polarized phonon modes (L and T_{xy}), the lowest transverse mode corresponding to the motion of atoms along the normal to the ML plane (T_z) is softened noticeably, especially toward the zone center where it is very shallow (see the inset in figure 10). Such a behavior results from the broken bonds in this direction, because the dynamical properties of atoms depend strongly on their bonding environment. As is shown for the alkaline earth metal MLs, Be(0001) and Mg(0001) [75, 76], the contribution of such soft phonons to the e–ph coupling is larger than that in the case of surfaces. In figure 10, the Eliashberg function averaged over momenta at the Fermi energy, $\alpha^2 F(\omega)$, and the phonon DOS, $F(\omega)$, for an ML of Mg(0001) are shown. Though the main features of $\alpha^2 F(\omega)$ are determined to a large extent by $F(\omega)$, the two functions are different. Unlike bulk Mg [77] or the Mg(0001) surface [76] and the Be(0001) ML, where low-energy and high-energy phonon modes participate equally in the e–ph coupling, the phonon spectrum of the Mg(0001) ML is substantially suppressed by e–ph matrix elements except for a prominent peak at low energies, 6–8 meV. The phonon modes giving the predominant contribution to the coupling with electronic states correspond to the previously mentioned perpendicular vibrations (T_z) with rather large wavevectors. A broad peak in the phonon DOS related to the zone center shallow part of the transverse phonon mode is completely suppressed and does not give any contribution to the e–ph scattering at all. For

both MLs considered, the strength of the e–ph coupling averaged over momenta at the Fermi energy is larger than the corresponding value in bulk or at the surface. In the Be(0001) ML $\lambda(E_F) = 0.51$, at the Be(0001) surface $\lambda(E_F) = 0.44$ and both values are significantly larger than $\lambda = 0.21$ evaluated at E_F of bulk Be [107]. The same situation is observed for a Mg(0001) ML, where $\lambda(E_F) = 0.58$ is twice as large than $\lambda(E_F)$ in bulk Mg [77].

5. Conclusion

A brief conclusion from these examples is that the e–ph coupling strength for these simple systems is now reasonably well understood. *Ab initio* calculations are of such a high quality that they compare well with the available experimental data. From the experimental side, extracting information on the e–ph interaction from the data is not straightforward and the choice of approach depends on the properties of the system (coupling strength and Debye temperature). The biggest challenge for the experiment is to provide data of sufficient quality to extract fine structure in the self-energy, which can then be related to individual phonon modes contributing to the e–ph coupling. Ideally, it would be possible to compare the fine structure in measured and calculated Eliashberg functions.

Acknowledgments

Financial support from the Lundbeck Foundation, the University of the Basque Country (GIC07IT36607), the Departamento de Educación del Gobierno Vasco and the Spanish Ministerio de Ciencia y Tecnologáa (MCyT) (Grant no. FIS200766711C0101) is gratefully acknowledged. We also thank G Benedek, K-P Bohnen, P M Echenique, A Eiguren, S V Eremeev, R Heid, B Hellsing and A Leonardo for enjoyable collaboration and discussions.

References

[1] Agergaard S, Søndergaard C, Li H, Nielsen M B, Hoffmann S V, Li Z and Hofmann Ph 2001 The effect of reduced dimensionality on a semimetal: the electronic structure of the Bi(110) surface *New J. Phys.* **3** 15.1–5.10

[2] Allen P B and Cohen M L 1969 Pseudopotential calculation of mass enhancement and superconducting transition temperature of simple metals *Phys. Rev.* **187** 525

[3] Anderson P W, Lee P A, Randeria M, Rice T M, Trivedi N and Zhang F C 2004 The physics behind high-temperature superconducting cuprates: the 'plain vanilla' version of rvb *J. Phys.: Condens. Matter* **16** R755

[4] Anderson P W and Schrieffer J R R 1991 A dialouge on the theory of high T_c *Phys. Today* **44** 54–61

[5] Ashcroft N W 1966 Electron–ion pseudopotentials in metals *Phys. Lett.* **23** 48

[6] Ast C R and Höchst H 2001 Fermi surface of Bi(111) measured by photoemission spectroscopy *Phys. Rev. Lett.* **87** 177602

[7] Ast C R and Höchst H 2002 Two-dimensional band structure and self-energy of Bi(111) near the $\bar{\Gamma}$ point. *Phys. Rev.* B **66** 125103

[8] Balasubramanian T, Glans P-A and Johansson L I 2000 Electron–phonon mass-enhancement parameter and the Fermi-line eccentricity at the Be(10$\bar{1}$0) surface from angle-resolved photoemission *Phys. Rev.* B **61** 12709–12

[9] Balasubramanian T, Jensen E, Wu X L and Hulbert S L 1998 Large value of the electron–phonon coupling parameter (λ=1.15) and the possibility of surface superconductivity at the Be(0001) surface *Phys. Rev.* B **57** R6866–9

[10] Baroni S, Giannozzi P and Tesla A 1987 Green's-function approach to linear response in solids *Phys. Rev. Lett.* **58** 1861–4
[11] Bartynski R A, Jensen E, Gustafsson T and Plummer E W 1985 Angle-resolved photoemission investigation of the electronic structure of Be: surface states *Phys. Rev.* B **32** 1921–6
[12] Bauer R, Schmid A, Pavone P and Strauch D 1998 Electron–phonon coupling in the metallic elements Al, Au, Na and Nb: a first-principles study *Phys. Rev.* B **57** 11276–82
[13] Borisova S D, Rusina G G, Eremeev S V, Benedek G, Echenique P M, Sklyadneva I Yu and Chulkov E V 2006 Vibrations in submonolayer structures of Na on Cu(111) *Phys. Rev.* B **74** 165412
[14] Brun C, Hong I-Po, Patthey F, Sklyadneva I Yu, Heid R, Echenique P M, Bohnen K-P, Chulkov E V and Schneider W-D 2009 Reduction of the superconducting gap of ultrathin Pb islands grown on Si(111) *Phys. Rev. Lett.* **102** 207002
[15] Carlsson A, Hellsing B, Lindgren S A and Wallden L 1997 High-resolution photoemission from a tunable quantum well: Cu(111)/Na *Phys. Rev.* B **56** 1593–600
[16] Chiang T C 2000 Photoemission studies of quantum well states in thin films *Surf. Sci. Rep.* **39** 181–235
[17] Chien T Y, Rienks E, Jensen M F, Hofmann Ph and Plummer E W to be published
[18] Chulkov E V, Borisov A G, Gauyacq J P, Sanchez-Portal D, Silkin V M, Zhukov V P and Echenique P M 2006 Electronic excitations in metals and at metal surfaces *Chem. Rev.* **106** 4160–206
[19] Chulkov E V, Kliewer J, Berndt R, Silkin V M, Hellsing B, Crampin S and Echenique P M 2003 Hole dynamics in a quantum-well state at Na/Cu(111) *Phys. Rev.* B **68** 195422
[20] Chulkov E V, Sarria I, Silkin V M, Pitarke J M and Echenique P M 1998 Lifetime of image-potential states on copper surfaces *Phys. Rev. Lett.* **80** 4947
[21] Chulkov E V, Silkin V M and Echenique P M 1997 Image potential states on lithium, copper and silver surfaces *Surf. Sci.* **391** L1217–23
[22] Chulkov E V, Silkin V M and Echenique P M 1999 Image potential states on metal surfaces: binding energies and wave functions *Surf. Sci.* **437** 330
[23] Cohen R E, Picket P W and Krakauer N 1990 Theoretical determination of strong electron–phonon coupling in $YBa_2Cu_3O_7$ *Phys. Rev. Lett.* **64** 2575–8
[24] Corriol C, Silkin V M, Sánchez-Portal D, Arnau A, Chulkov E V, Echenique P M T, von Hofe, Kliewer J, Kröger J and Berndt R 2005 Role of elastic scattering in electron dynamics at ordered alkali ovelayeres on Cu(111) *Phys. Rev. Lett.* **95** 176802
[25] Dacorogna M M, Cohen M L and Lam P K 1985 Self-consistent calculation of the electron–phonon coupling in aluminium *Phys. Rev. Lett.* **55** 837–40
[26] Damascelli A, Hussain Z and Shen Z-X 2003 Ange-resolved photoemission studies of the cuprate supercondcuctors *Rev. Mod. Phys.* **75** 473
[27] Devreese J T, Van V E Doren and Van Camp P E 1983 *Ab initio Calculations of Phonon Spectra* (New York: Plenum)
[28] Black J E, Shanes F C and Wallis R F 1983 Surface vibrations on face-centered cubic metal-surfaces—the (111) surfaces *Surf. Sci.* **133** 199–215
[29] Eberhardt W and Plummer E W 1980 Angle-resolved photoemission determination of the band structure and multielectron excitations in Ni *Phys. Rev.* B **21** 3245–55
[30] Echenique P M, Berndt R, Chulkov E V, Fauster Th, Goldmann A and Höfer U 2004 Decay of electronic excitations at metal surfaces *Surf. Sci. Rep.* **52** 219
[31] Eiguren A, Hellsing B, Chulkov E V and Echenique P M 2003 Phonon-mediated image state electron decay of metal surfaces *J. Electron Spectrosc. Related Phenom.* **129** 111
[32] Eiguren A, de Gironcoli S, Chulkov E V, Echenique P M and Tosatti E 2003 Electron–phonon interaction at the Be(0001) surface *Phys. Rev. Lett.* **91** 166803
[33] Eiguren A, Hellsing B, Chulkov E V and Echenique P M 2003 Phonon-mediated decay of metal surface states *Phys. Rev.* B **67** 235423

[34] Eiguren A, Hellsing B, Reinert F, Nicolay G, Chulkov E V, Silkin V M, Hüfner S and Echenique P M 2002 Role of bulk and surface phonons in the decay of metal surface states *Phys. Rev. Lett.* **88** 066805
[35] Eiguren A and Ambrosch-Draxl C 2008 Wannier interpolation scheme for phonon-induced potentials: application to bulk MgB_2, W and the (1×1) H-covered W(110) surface *Phys. Rev.* B **78** 045124
[36] Engelsberg S and Schrieffer J R 1963 Coupled electron–phonon systems *Phys. Rev.* **131** 993–1008
[37] Eremeev S V, Rusina G G, Borisova S D and Chulkov E V 2008 Electron–phonon interaction in the quantum well state of the 1 ML Na/Cu(111) system *Fiz. Tverd. Tela* **50** 311–6
[38] Eremeev S V, Sklyadneva I Yu, Echenique P M, Borisova S D, Benedek G, Rusina G G and Chulkov E V 2007 Electron–phonon coupling in a sodium monolayer on Cu(111) *Surf. Sci.* **601** 4553–6
Eremeev S V, Sklyadneva I Yu, Echenique P M, Borisova S D, Benedek G, Rusina G G and Chulkov E V 2006 *24th European Conf. on Surface Science (ECOSS-24) (Paris, France, 4–8 September)*
[39] Rienks E D L *et al* to be published
[40] Fischer N, Schuppler S, Fischer R, Fauserter T and Steinmann W 1991 Electronic-structure of a single layer of Na on Cu(111) *Phys. Rev.* B **43** 14722–5
[41] Gartland P O and Slagsvold B J 1975 Transitions conserving parallel momentum in photoemission from the (111) face of copper *Phys. Rev.* B **12** 4047–58
[42] Gayone J E, Hoffmann S V, Li Z and Hofmann Ph 2003 Strong energy dependence of the electron–phonon coupling on Bi(100) *Phys. Rev. Lett.* **91** 127601
[43] Gayone J E, Kirkegaard C, Wells J W, Hoffmann S V, Li Z and Hofmann Ph 2005 Determining the electron–phonon mass enhancement parameter λ on metal surfaces *Appl. Phys.* A **80** 943–9
[44] Grimvall G 1981 *The Electron–Phonon Interaction in Metals* (Amsterdam: North-Holland)
[45] Guo Y *et al* 2004 Superconductivity modulated by quantum size effects *Science* **306** 1915–7
[46] Hansen E D, Miller T and Chiang T-C 1998 Observation of photoemission line widths narrower than the inverse lifetime *Phys. Rev. Lett.* **80** 1766–9
[47] Heimann P, Neddermeyer H and Roloff H F 1977 Ultraviolet photoemission from intrinsic surface-states of noble-metals *J. Phys. C: Solid State Phys.* **10** L17–22
[48] Hellsing B, Carlsson J, Wallden L and Lindgren S A 2000 Phonon-induced decay of a quantum-well hole: one monolayer Na on Cu(111) *Phys. Rev.* B **61** 2343–8
[49] Hellsing B, Eiguren A and Chulkov E V 2002 Electron–phonon coupling at metal surfaces *J. Phys.: Condens. Matter* **14** 5959–77
[50] Hengsberger M, Frésard R, Purdie D, Segovia P and Baer Y 1999 Electron–phonon coupling in photoemission spectra *Phys. Rev.* B **60** 10796–802
[51] Hengsberger M, Purdie D, Segovia P, Garnier M and Baer Y 1999 Photoemission study of a strongly coupled electron–phonon system *Phys. Rev. Lett.* **83** 592–5
[52] Hengsberger M, Segovia P, Garnier M, Purdie D and Baer Y 2000 Photoemission study of the carrier bands in Bi(111) *Eur. Phys. J.* B **17** 603–8
[53] Höchst H and Ast C R 2004 The fermi surfaces of thin Sb(111) films *J. Electron Spectrosc. Relat. Phenom.* **137–140** 441
[54] Hofer U, Shumay I L, Reuss Ch, Thomann U, Wallauer W and Fauster Th 1997 Time-resolved coherent photoelectron spectroscopy of quantized electronic states on metal surfaces *Science* **277** 1480–2
[55] Hofmann Ph 2006 The surfaces of bismuth: structural and electronic properties *Prog. Surf. Sci.* **81** 191–245
[56] Hofmann Ph, Cai Y Q, Grütter C and Bilgram J H 1998 Electron–lattice interactions on α-Ga(010) *Phys. Rev. Lett.* **81** 1670–3
[57] Hofmann Ph, Gayone J E, Bihlmayer G, Koroteev Yu M and Chulkov E V 2005 The electronic structure and fermi surface of Bi(100) *Phys. Rev.* B **71** 195413
[58] Hsieh D, Qian D, Wray L, Xia Y, Hor Y S, Cava R J and Hasan M Z 2008 A topological Dirac insulator in a quantum spin hall phase *Nature* **452** 970–4
[59] Hsieh D *et al* 2009 Observation of unconventional quantum spin textures in topological insulators *Science* **323** 919–22

[60] Hüfner S 2003 *Photoelectron Spectroscopy* 3rd edn (Berlin: Springer)
[61] Hulbert S L, Johnson P D, Stoffel N G and Smith N V 1985 Unoccupied bulk and surface-states on Ag(111) studied by inverse photoemission *Phys. Rev.* B **32** 3451–5
[62] Fuglsang M Jensen, Kim T K, Bengio S, Yu Sklyadneva I, Leonardo A, Eremeev S V, Chulkov E V and Hofmann Ph 2007 Thermally induced defects and the lifetime of electronic surface states *Phys. Rev.* B **75** 153404
[63] Kevan S D (ed) 1992 Angle-resolved Photoemission *Studies in Surface Chemistry and Catalysis* vol 74 (Amsterdam: Elsevier)
[64] Kim T K, Sorensen T S, Wolfring E, Li H, Chulkov E V and Hofmann Ph 2005 Electron–phonon coupling on the Mg(0001) surface *Phys. Rev.* B **72** 075422
[65] Kirkegaard C, Kim T K and Hofmann Ph 2005 Self-energy determination and electron–phonon coupling on Bi(110) *New J. Phys.* **7** 99
[66] Kliewer J and Berndt R 2002 Scanning tunneling spectroscopy of Na on Cu(111) *Phys. Rev.* B **65** 035412
[67] Kliewer J, Berndt R, Chulkov E V, Silkin V M, Echenique P M and Crampin S 2000 Dimensionality effects in the lifetime of surface states *Science* **288** 1399–402
[68] Kordyuk A A, Borisenko S V, Koitzsch A, Fink J, Knupfer M and Berger H 2005 Bare electron dispersion from experiment: self-consistent self-energy analysis of photoemission data *Phys. Rev.* B **71** 214513
[69] Koroteev Yu M, Bihlmayer G, Gayone J E, Chulkov E V, Blügel S, Echenique P M and Hofmann Ph 2004 Strong spin–orbit splitting on bi surfaces *Phys. Rev. Lett.* **93** 046403
[70] Kroger J, Limot L, Jensen H, Berndt R, Crampin S and Pehlke E 2005 Surface state electron dynamics of clean and adsorbate-covered metal surfaces studied with the scanning tunnelling microscope *Prog. Surf. Sci.* **80** 26–48
[71] Kroger J 2006 Electron–phonon coupling at metal surfaces *Rep. Prog. Phys.* **69** 899–969
[72] Lanzara A *et al* 2001 Evidence for ubiquitous strong electron–phonon coupling in high-temperature superconductors *Nature* **412** 510–4
[73] LaShell S, Jensen E and Balasubramanian T 2000 Nonquasiparticle structure in the photoemission spectra from the Be(0001) surface and determination of the electron self energy *Phys. Rev.* B **61** 2371–4
[74] LaShell S, McDougall B A and Jensen E 2006 Electron–phonon mass enhancement parameter of the [overline gamma] surface state on Au(111) measured by photoemission spectroscopy *Phys. Rev.* B **74** 033410
[75] Leonardo A, Sklyadneva I Yu, Echenique P M and Chulkov E V 2006 Electron–phonon interaction in a free standing beryllium monolayer *Surf. Sci.* **600** 3715–7
Leonardo A, Sklyadneva I Yu, Echenique P M and Chulkov E V 2005 *23rd European Conf. on Surface Science (ECOSS-23) (Berlin, Germany, 4–9 September)*
[76] Leonardo A, Sklyadneva I Yu, Echenique P M and Chulkov E V 2007 Electron–phonon interaction in magnesium: from the monolayer to the Mg(0001) surface *Surf. Sci.* **601** 4018–21
[77] Leonardo A, Sklyadneva I Yu, Silkin V M, Echenique P M and Chulkov E V 2007 *Ab initio* calculation of the phonon-induced contribution to the electron-state linewidth on the Mg(0001) surface versus bulk Mg *Phys. Rev.* B **76** 035404
[78] Levinson H J, Greuter F and Plummer E W 1983 Experimental bandstructure of aluminium *Phys. Rev.* B **27** 727–47
[79] Liechtenstein A I, Mazin I I, Rodriguez C O, Jepsen O, Andersen O K and Methfessel M Structural phase diagram and electron–phonon interaction in $Ba_{1-x}K_xBiO_3$ *Phys. Rev.* B **44** 5388–91
[80] Liu AY and Quong A A 1996 Linear-response calculation of electron–phonon coupling parameters *Phys. Rev.* B **53** R7575–9
[81] Liu Y and Allen R E 1995 Electronic structure of the semimetals Bi and Sb *Phys. Rev.* B **52** 1566
[82] Luh D-A, Miller T, Paggel J J and Chiang T-C 2002 Large electron–phonon coupling at an interface *Phys. Rev. Lett.* **88** 256802
[83] Mathias S, Wiesenmayer M, Aeschlimann M and Bauer M 2006 Quantum-well wave-function localization and the electron–phonon interaction in thin Ag nanofilms *Phys. Rev. Lett.* **97** 236809

[84] Mathias S, Eremeev S-V, Chulkov E-V, Aeschlimann M and Bauer M 2009 Quantum oscillation in coupled two-dimensional electron system *Phys. Rev. Lett.* **103** 026802
[85] Matzdorf R 1998 Investigation of line shapes and line intensities by high-resolution UV-photoemission spectroscopy—some case studies on noble-metal surfaces *Surf. Sci. Rep.* **30** 153–206
[86] Matzdorf R, Meister G and Goldmann A 1996 Phonon contriubtions to photohole linewidth observed for surface states on copper *Phys. Rev.* B **54** 14807
[87] McDougall B A, Balasubramanian T and Jensen E 1995 Phonon contribution to quasiparticle lifetimes in Cu measured by angle-resolved photoemission *Phys. Rev.* B **51** R13891
[88] McMillan W L 1968 Transition temperature of strong-coupled superconductors *Phys. Rev.* **167** 331–4
[89] Milun M, Pervan P and Woodruff D P 2002 Quantum well structures in thin metal films: simple model physics in reality? *Rep. Prog. Phys.* **65** 99–141
[90] Nojima A, Yamashita K and Hellsing B 2008 Model Eliashberg function for surface states *Appl. Surf. Sci.* **254** 7938–41
[91] Osma J, Sarría I, Chulkov E-V, Pitarke I-M and Echenique P-M 1999 Role of intrinsic surface state in the decay of image states at a metal surface *Phys. Rev.* B **59** 10591–8
[92] Paggel J J, Luh D-A, Miller T and Chiang T-C 2004 Electronic-structure dependence of the electron–phonon interaction in Ag *Phys. Rev. Lett.* **92** 186803
[93] Paggel J J, Miller T and Chiang T-C 1999 Temperature dependent complex band structure and electron–phonon coupling in Ag *Phys. Rev. Lett.* **83** 1415–8
[94] Plummer E W 1985 Deficiencies in the single particle picture of valence band photoemission *Surf. Sci.* **152/153** 162–79
[95] Plummer E W and Hannon J B 1994 The surfaces of beryllium *Prog. Surf. Sci.* **46** 149
[96] Reinert F, Nicolay G, Schmidt S, Ehm D and Hüfner S 2001 Direct measurements of the L-gap surface states on the (111) face of noble metals by photoelectron spectroscopy *Phys. Rev.* B **63** 115415
[97] Reutt J E, Chabal Y J and Christman S B 1998 Coupling of H vibration to substrate electronic states in Mo(100)-p(1 × 1)H and W(100)-p(1 × 1)H: example of strong breakdown of adiabaticity *Phys. Rev.* B **38** 3112
[98] Rotenberg E and Kevan S D 2002 Electron–phonon coupling in w(111)-(1 × 1)h *J. Electron Spectrosc. Relat. Phenom.* **126** 125
[99] Rotenberg E, Schaefer J and Kevan S D 2000 Coupling between adsorbate vibrations and an electronic surface state *Phys. Rev. Lett.* **84** 2925–8
[100] Sarría I, Osma J, Chulkov E V, Pitarke J M and Echenique P M 1999 Self-energy of image states on copper surfaces *Phys. Rev.* B **60** 11795–803
[101] Savrasov S Y, Savrasov D Y and Andersen O K 1994 Linear-response calculations of electron–phonon interactions *Phys. Rev. Lett.* **71** 372–5
[102] Savrasov S Y and Savrasov D Y 1996 Electron–phonon interactions and related physical properties of metals from linear-response theory *Phys. Rev.* B **54** 16487–501
[103] Schiller F, Heber M, Servedio V D P and Laubschat C 2004 Electronic structure of Mg: from monolayers to bulk *Phys. Rev.* B **70** 125106
[104] Shi J *et al* 2004 Direct extraction of the Eliashberg function for electron–phonon coupling: a case study of be(10$\bar{1}$0) *Phys. Rev. Lett.* **92** 186401
[105] Silkin V M, Balasubramanian T, Chulkov E V, Rubio A and Echenique P M 2001 Surface-state hole decay mechanisms: the Be(0001) surface *Phys. Rev.* B **6408** 085334
[106] Sklyadneva I, Yu Chulkov E V and Echenique P M 2008 Electron–phonon interaction on an Al(001) surface *J. Phys. Condens. Matter* **20** 165203
[107] Sklyadneva I, Yu Chulkov E V, Schöne W-D, Silkin V M, Keyling R and Echenique P M 2005 Role of electron–phonon interactions versus electron–electron interactions in the broadening mechanism of the electron and hole linewidths in bulk Be *Phys. Rev.* B **71** 174302

[108] Sklyadneva I Yu, Leonardo A, Echenique P M, Eremeev S V and Chulkov E V 2006 Electron–phonon contribution to the phonon and excited electron (hole) linewidths in bulk Pd *J. Phys. Condens. Matter* **18** 7923–35

[109] Smith N V, Thiry P and Petroff Y 1993 Photoemission linewidth and quasiparticle lifetimes *Phys. Rev.* B **47** 15476–81

[110] Sugawara K, Sato T, Souma S, Takahashi T, Arai M and Sasaki T 2006 Fermi surface and anisotropic spin–orbit coupling of Sb(111) studied by angle-resolved photoemission spectroscopy *Phys. Rev. Lett.* **96** 046411–4

[111] Tang S J, Ismail, Sprunger P T and Plummer E W 2002 Electron–phonon coupling and temperature-dependent shift of surface state on Be($10\bar{1}0$) *Phys. Rev.* B **65** 235428

[112] Tang S-J *et al* 2004 A spectroscopic view of electron–phonon coupling at metal surfaces *Phys. Status Solidi* b **241** 2345–52

[113] Teo J C Y, Fu L and Kane C L 2008 Surface states and topological invariants in three-dimensional topological insulators: application to $Bi_{1-x}Sb_x$ *Phys. Rev.* B **78** 045426

[114] Valla T, Fedorov A V, Johnson P D and Hulbert S L 1999 Many-body effects in angle-resolved photoemission: quasiparticle energy and lifetime of a Mo(110) surface state *Phys. Rev. Lett.* **83** 2085–8

[115] Vitali L, Wahl P, Schneider M A, Kern K, Silkin V M, Chulkov E V and Echenique P M 2003 Inter- and intraband inelastic scattering of hot surface state electrons at the Ag(111) surface *Surf. Sci.* **523** L47–52

[116] Weinelt M 2002 Time-resolved two-photon photoemission from metal surfaces *J. Phys. Condens. Matter* **14** R1099–141

[117] Wells J W *et al* 2009 Nondegenerate metallic states on Bi(114): a one-dimensional topological metal *Phys. Rev. Lett.* **102** 096802

[118] Winter H 1981 Application of linear response theory to electron–phonon coupling *J. Phys. F: Metal Phys.* **11** 2283–300

[119] Yan J-A, Ruan W Y and Chou M Y 2009 Electron–phonon interaction for optical-phonon modes in few-layer graphene: first-principles calculations *Phys. Rev.* B **79** 115443

[120] Yarnell J L, Warren J L, Wenzel R G and Koenig S H 1964 Phonon dispersion curves in bismuth *IBM J. Res. Dev.* **8** 234

[121] Zein N E 1984 *Sov. Phys. Solid State* **26** 3028

[122] Zhang Y F, Jia J F, Han T Z, Tang Z, Shen Q T, Guo Y, Qiu Z Q and Xue Q K 2005 Band structure and oscillatory electron–phonon coupling of Pb thin films determined by atomic-layer-resolved quantum-well states *Phys. Rev. Lett.* **95** 096802